Non-reciprocal transmission and Schmitt trigger operation in strongly modulated asymmetric WBGs

Masafumi Fujii, Ayan Maitra[†], Christopher Poulton[††], Juerg Leuthold[†], and Wolfgang Freude[†]

Department of Electrical, Electronic and System Engineering, University of Toyama, 3190 Gofuku, Toyama, 930-8555 Japan

[†]*Institute of High-Frequency and Quantum Electronics (IHQ), University of Karlsruhe, 76131 Karlsruhe, Germany*

[††]*Max-Planck Research Group for Optics, Information and Photonics, University of Erlangen-Nuremberg, Guenther-Scharowsky-Str. 1 / Bau 24, D-91058, Erlangen, Germany.*

mfujii@eng.u-toyama.ac.jp

Abstract: We investigate numerically a non-reciprocal switching behavior in strongly modulated waveguide Bragg gratings (WBGs) having a longitudinally asymmetric stopband configuration. The minimum power predicted for a stable switching operation is found to be approximately 77 mW for a realistic waveguide structure made of prospective materials; we assume in this paper a nano-strip InGaAsP/InP waveguide having longitudinally asymmetric modulation of the waveguide width. The analysis has been performed with our in-house nonlinear finite-difference time-domain (FDTD) code adapted to parallel computing. The numerical results clearly show low-threshold Schmitt trigger operation, as well as non-reciprocal transmission property where the switching threshold for one propagation direction is lower than that for the other direction. In addition, we discuss the modulation-like instability phenomena in such nonlinear periodic devices by employing both an instantaneous Kerr nonlinearity and a more involved saturable nonlinearity model.

OCIS codes: (130.4310) nonlinear integrated optics; (190.1450) bistability

References and links

1. M.D.Tocci, M.J.Bloemer, M.Scalora, J.P.Dowling, and C.M.Bowden, "Thin-film nonlinear optical diode," Appl. Phys. Lett. **66**, 2324–2326 (1995).
2. A.Maitra, C.G.Poulton, J.Wang, J.Leuthold, and W.Freude, "Low switching threshold using nonlinearities in stopband-tapered waveguide Bragg gratings," IEEE J. Quantum Electron. **41**, 1303–1308 (2005).
3. W. Freude, A. Maitra, J. Wang, C. Koos, C. Poulton, M. Fujii, and J. Leuthold, "All-optical signal processing with nonlinear resonant devices," in *Proc. 8th Intern. Conf. on Transparent Optical Networks (ICTON'06)*, Vol. 2, (Nottingham, UK, 2006), paper We.D2.1, pp. 215-219.
4. W.Chen and D.L.Mills, "Gap solitons and the nonlinear optical response of superlattices," Phys. Rev. Lett. **58**, 160–163 (1987).
5. C. de Sterke and J.E.Sipe, "Switching dynamics of finite periodic nonlinear media: A numerical study," Phys. Rev. A **42**, 2858–2869 (1990).
6. C. Sterke and J.E.Sipe, "Gap solitons," in *Progress in Optics*, vol.XXXIII, pp.203-260, North-Holland, Amsterdam (1994).

#77312 - $15.00 USD Received 21 November 2006; revised 12 December 2006; accepted 13 December 2006

7. M.Scalora, J.P.Dowling, C.M.Bowden, and M.J.Bloemer, "Optical limiting and switching of ultrashort pulses in nonlinear photonic band gap materials," Phys. Rev. Lett. **73**, 1368–1371 (1994).
8. M.W.Feise, I.V.Shdrivov, and Y.S.Kivshar, "Bistable diode action in left-handed periodic structures," Phys. Rev. E **71**, 037,602 (2005).
9. X-H.Jia, Z-M.Wu, and G-Q.Xia, "Analysis of bistable steady characteristics and dynamic stability of linearly tapered nonlinear Bragg gratings," Opt. Express **12**, 2945–2953 (2004).
10. E.Lidorikis and C.M.Soukoulis, "Pulse-driven switching in one-dimensional nonlinear photonic band gap materials: a numerical study," Phys. Rev. E **61**, 5825–5829 (2000).
11. X.-S.Lin and S.Lan, "Unidirectional transmission in asymmetrically confined photonic crystal defects with Kerr nonlinearity," Chin. Phys. Lett. **22**, 2847–2850 (2005).
12. M.Notomi, A.Shinya, S.Mitsugi, G.Kira, E.Kuramochi, and T.Tanabe, "Optical bistable switching action of Si high-Q photonic-crystal nanocavities," Opt. Express **13**, 2678–2687 (2005).
13. O.H.Schmitt, "A thermionic trigger," J. Scientific Instruments **15**, 24 (1938).
14. M.Fujii, C.Koos, C.Poulton, J.Leuthold, and W.Freude, "Nonlinear FDTD analysis and experimental verification of four-wave mixing in InGaAsP/InP racetrack micro-resonators," IEEE Photon. Technol. Lett. **18**, 361–363 (2006).
15. C.Koos, M.Fujii, C.Poulton, R.Steingrueber, J.Leuthold, and W.Freude, "FDTD-modeling of dispersive nonlinear ring resonators: Accuracy studies and experiments," IEEE J. Quantum Electron. In print.
16. J.Koga, "Simulation model for the effects of nonlinear polarization on the propagation of intense pulse lasers," Optics Lett. **24**, 408–410 (1999).
17. K.S.Yee, "Numerical solution of initial boundary value problems involving Maxwell's equation in isotropic media," IEEE Trans. Antennas Prop. **14**, 302–307 (1966).
18. M.Fujii, M.Tahara, I.Sakagami, W.Freude, and P.Russer, "High-order FDTD and auxiliary differential equation formulation of optical pulse propagation in 2D Kerr and Raman nonlinear dispersive media," IEEE J. Quantum Electron. **40**(2), 175–182 (2004).
19. A.Taflove and S.C.Hagness, *Computational electrodynamics: The finite-difference time-domain method, 3rd ed.*, chap. 9 (Artech House, 2005).

1. Introduction

Compact and integrated optical devices are of particular importance for the realization of faster and more affordable communication technologies. Among various optical devices, all-optical switches and logic gates are the key components for the ultra-fast optical signal processing [1, 2, 3]. It is well known that these functionalities are realized by optical bistability in periodic nonlinear media [4, 5, 6, 7, 8] and its asymmetric variations [9]. However, previous literature address one-dimensional (1D) simple structures having weak perturbation, and those analyzed by either a transfer-matrix method or coupled mode equations.

Some authors apply the pseudo-spectral time domain method to a 1D left-handed multilayer system [8]. Others apply the nonlinear finite-difference time-domain (FDTD) method to a 1D weakly modulated multilayer structure [10], and also to asymmetrically arranged photonic crystal defects in a slab waveguide [11]. However, the light intensity required for the nonlinear switching operation is nevertheless found still orders of magnitude higher than are in real with widely available experimental setups. Recently, very low switching-threshold operation has been achieved in a photonic crystal bistable nanocavities by employing two-photon absorption (TPA) in Si [12]. A disadvantage of TPA is that the switching speed is much slower than that of the nonlinearity of electronic origin [6]. It would therefore be desirable to clarify possible conditions with which minimum switching power is achieved for particular realistic device structures and materials while retaining a sufficient speed of operation.

In this paper we investigate numerically an optical Schmitt trigger [13] operation in a longitudinally asymmetric WBG. These WBGs have also the property of non-reciprocal transmission where the switching threshold in one direction is lower than that in the other direction. The analyzed WBG has a structure that can be actually fabricated by employing an optical planar circuit technology based on a InGaAsP/InP system with strong nonlinearity [14, 15]. The sidewall modulation of this structure is strong, and the coupled mode equations may not be directly applied due to the strong coupling between the forward and the backward waves [6, 2].

#77312 - $15.00 USD Received 21 November 2006; revised 12 December 2006; accepted 13 December 2006

Therefore, analysis has been performed fully numerically with the nonlinear finite-difference time-domain (FDTD) method that inherently deals with the necessary coupling and guiding effects of the WBGs; the code has been developed by the authors, and it runs effectively on parallel cluster computers [14]. Some authors have addressed an instability issue in nonlinear periodic structures [6, 9, 8]. In this respect we have investigated the field inside the grating using either the simple optical Kerr nonlinearity and damped Lorentz dispersion [14, 15], or the soft-core Coulomb potential as a stable numerical model of the saturable nonlinear mechanism of bound electrons [16]. The behavior of the chaotic states in the nonlinear WBG is discussed qualitatively.

2. Numerical Experiment

2.1. Asymmetric waveguide Bragg grating

The asymmetric WBG has been modeled such that the stopband of the grating has a nearly linear profile along the waveguide. The grating is realized by a sidewall periodic perturbation of a dielectric waveguide whose top view and cross section are shown in Figs. 1(a) and (b), respectively. The sidewall modulation is expressed by a function of distance z as

$$x(z) = \pm \left[\frac{W}{2} + \frac{W_g}{2} g(z/L_0) \sin\left(\frac{2\pi z}{\Lambda} \right) \right] , \tag{1}$$

where Λ is the period of the grating chosen to be $\Lambda = 0.241\mu$m for this paper, and L_0 is the total length of the grating. The averaged width of the waveguide was chosen to be $W = 0.4$ μm such that it supports only the dominant propagation mode at the operating frequency. The maximum amplitude of the sidewall modulation is determined by $W_g/2$. The nearly linear variation of the band edge frequency is described by a 3rd-order polynomial in terms of the normalized distance $z' = z/L_0$ as $g(z') = az'^3 + bz'^2 + cz' + d$, whose coefficients have been found by fitting the polynomial to some FDTD results of stopbands for uniform waveguide gratings as shown in Fig. 2; they are chosen to be $a = -0.4856$, $b = -0.0009$, $c = 0$, and $d = 1$, and the resulting profile of the upper band-edge frequency for $W_g = 0.1$ μm is shown in Fig. 1(c). With this profile the sidewall modulation amplitude varies nonlinearly from $W_g/2$ at the left-hand-side of the waveguide to $W_g/4$ at the right-hand-side of the waveguide.

For the numerical model, the actual variation of the band-gap frequency is approximated by a stair-cased finite-difference discretization. Due to the restriction of the computational resource, the cell sizes have been chosen to be $\Delta x = 0.025$ μm and $\Delta z = \Lambda/10 = 0.0241$ μm. Note that Δx is comparable to the side wall modulation, and it may appear too coarse to resolve the depth of the modulation. However, Δz is sufficiently small to resolve the periodic variation of the grating. We have therefore checked in preliminary analyses that the present cell size can resolve the side-wall modulation sufficiently for the purpose to realize the nearly linear profile of the band edge frequency.

We define the direction of light transmission as follows: when a light is transmitted from left to right (LTR), it goes through a waveguide having a negatively varying stopband (the stopband width is decreasing). In contrast, when light is transmitted from right to left (RTL), it goes through a waveguide having a positively varying stopband (the stopband width is increasing). We emphasize that the sidewall modulation chosen in this paper is much stronger than that in previous literature in order to reduce the length of the WBG and the required incident light power for switching.

The waveguide has a three-dimensional (3D) pedestal waveguide structure as in Fig. 1, which consists of InP (refractive index $n = 3.17$ at wavelength $\lambda = 1.55$ μm) for the upper and the lower cladding, InGaAsP ($n = 3.42$ at the same wavelength) for the core, and surrounding air. For the numerical representation, the structure is approximated by a dielectric slab of $n = 3.34$

#77312 - $15.00 USD Received 21 November 2006; revised 12 December 2006; accepted 13 December 2006

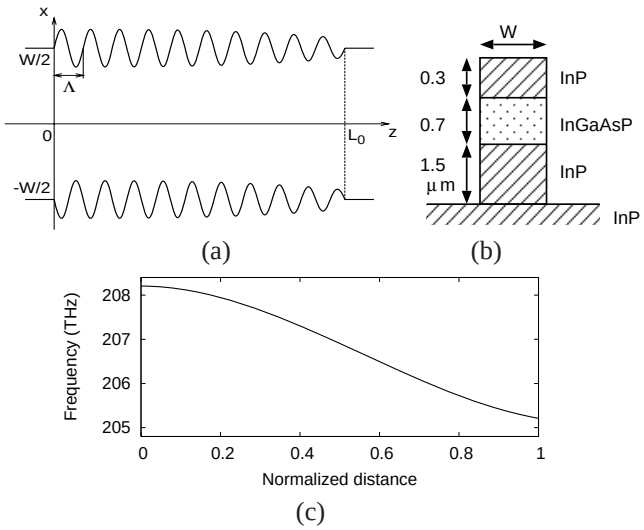

Fig. 1. Schematic configuration of the waveguide Bragg grating having an asymmetric stopband; (a) the top view, and (b) the cross section of the waveguide. In the analysis the structure is approximated by a slab waveguide having an effective refractive index of the stacked structure. The ports for signal detection are located at a half hight of the InGaAsP core and at $(x,z) = (0,0)$ and $(0,L_0)$. (c) An example of the upper band-edge frequency variation realized by the third-order polynomial $g(z')$ for $W_g = 0.1$ μm.

to be analyzed by a 2D FDTD method. The polarization of the incident light is quasi-TM where the dominant electric field component is perpendicular to the substrate. We employ the same fabrication and design procedures used in [14, 15]. The third-order nonlinear susceptibility for InGaAsP core has been confirmed to be $\chi_0^{(3)} = 3.8 \times 10^{-18}$ m^2/V^2 by our extensive numerical and experimental investigations [14, 15].

2.2. FDTD analysis of WBG

We apply Yee's FDTD algorithm to Maxwell's equations [17] including the constitutive equation of isotropic media with Kerr nonlinearity and typical chromatic dispersion properties through the auxiliary differential equation (ADE) technique [18, 19]. The optical Kerr nonlinearity is modeled with an instantaneous response, and TPA is not taken into consideration. When the incident light power is reduced to the level of 100 mW or less, this is considered to be an appropriate approximation. The relation between the field E and the light power P has been derived by numerically evaluating the effective area of the waveguide $A = 5.3 \times 10^{-13}$ m^2, thus we obtain $P = A|E|^2/(2\eta)$, where $\eta = 377\ \Omega$ is the intrinsic wave impedance of vacuum.

For the asymmetric WBG of $W_g = 0.1$ μm and $W_g = 0.2$ μm, the transmission spectra for weak incidence have been analyzed as shown in Fig. 3. It is clearly seen in this figure that each spectrum is the combined one of those found in Fig. 2 for uniform gratings; due to the asymmetric variation of the grating modulation, the total transmission is also asymmetric with respect to frequency. In the previous 1D model e.g. in [2], both the upper and the lower band-edges are changed while the stopband center remains unchanged. In contrast, for the present waveguide model the stopband center is chirped as well as that the upper band-edge changes largely. The operating frequency is generally chosen to be slightly lower than the upper band-edge frequency.

#77312 - $15.00 USD Received 21 November 2006; revised 12 December 2006; accepted 13 December 2006

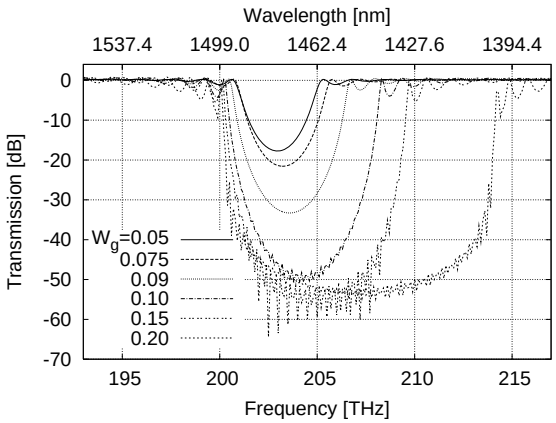

Fig. 2. Transmission spectra for the 100Λ-long waveguide Bragg gratings of uniform amplitudes of sidewall modulation. W_g in legend is in μm.

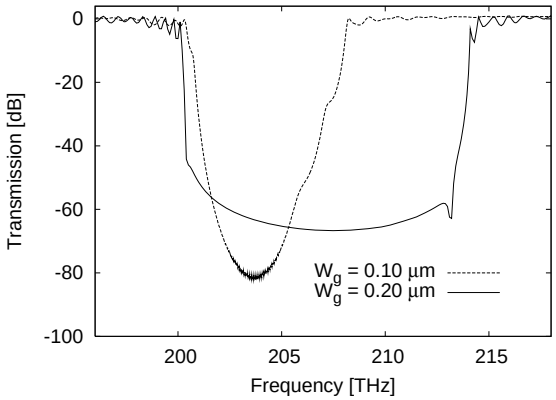

Fig. 3. Comparison of the calculated transmission spectra for 200-Λ-long asymmetric gratings with the maximum modulation $W_g = 0.1$ μm and $W_g = 0.20$ μm. The upper frequency band edges are 208.20 THz for $W_g = 0.1$ μm, and 214.08 THz for $W_g = 0.20$ μm.

We first chose the operating frequency at 207.9 THz (or free space wavelength $\lambda_0 = 1442$ nm) for the case of $W_g = 0.1$ μm, i.e. the frequency difference from the upper band edge was $\Delta f = 0.3$ THz, and launched a sinusoidal wave from either the left-hand-side or the right-hand-side port of the asymmetric WBG. The incident light power is gradually increased, followed by a flat region such that the field in the grating establishes a stationary state. This staircase-like input is repeatedly cumulated until the incident light becomes strong enough to cause switching, and then the incident power is reduced in a similar manner until it vanishes. This allows the detection of the switch-on and -off thresholds of the WBG. The incident and the output time signals are plotted in Fig. 4 for the WBG of $L_0 = 235\Lambda$; due to the rapidly oscillating sinusoidal carrier, only the envelopes of the incident and the output signals for the RTL and the LTR configurations are visible in the figure. It is observed that the switching threshold is lower for the RTL configuration than for the LTR configuration; the switch-on threshold of the electric field is $E_{th}^{(on)} = 2.6 \times 10^7$ V/m (equivalent light power $P_{th}^{(on)} = 480$ mW) for RTL, while it is

#77312 - $15.00 USD Received 21 November 2006; revised 12 December 2006; accepted 13 December 2006

$E_{th}^{(on)} = 3.7 \times 10^7$ V/m ($P_{th}^{(on)} = 950$ mW) for LTR. The switch-off threshold field is $E_{th}^{(off)} = 1.8 \times 10^7$ V/m ($P_{th}^{(off)} = 240$ mW) for RTL, while it is $E_{th}^{(off)} = 2.6 \times 10^7$ V/m ($P_{th}^{(off)} = 490$ mW) for LTR. Either of the two transmission plots show the Schmitt trigger operation, i.e. the switch turns on at a certain incident power, holding the on-state until the input passes through a lower threshold power [13]. Note also that the transition time for switching is 2 to 3 ps. Overshoot and bouncing are seen afterwards, and the signal settling time is approximately 10 ps. The right vertical axis of Fig. 4 shows the change in normalized permittivity by the optical Kerr nonlinearity, and this is convenient when the switching threshold is compared to other results. For this case the change in normalized permittivity for the switch-on threshold is 2.2×10^{-4}, which is much smaller than those used in literature, e.g. [4].

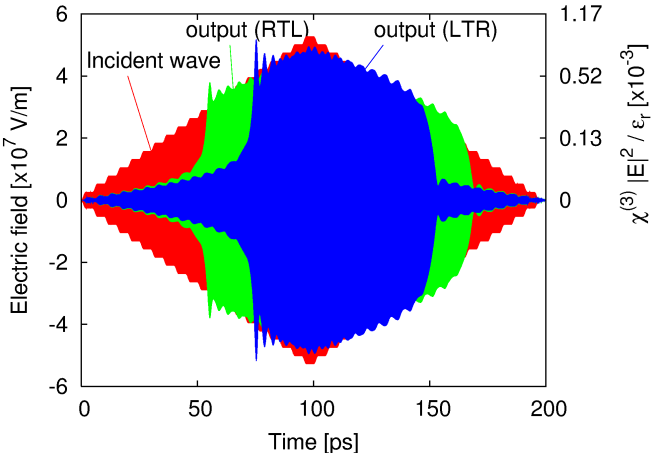

Fig. 4. Switching for the LTR and RTL configuration of a 235Λ-long waveguide with $W_g = 0.1$ μm at 207.9 THz operating frequency ($\Delta f = 0.3$ THz). Maximum incident field value is 5.25×10^7 V/m at 100 ps. Right vertical axis shows the normalized permittivity change by the nonlinearity.

The origin of the nonreciprocity and the stability is described qualitatively in [1, 9]; as in these references, the behavior of the field inside the grating is reasonably considered in view of energy diffusion. Due to the monotonic change of the band-edge frequency, for the LTR (negative) configuration, the light power injected into the grating diffuses gradually in the forward direction, which leads to a large power required for switching. In contrast for the RTL (positive) configuration, the incident light power can be built up within the grating since the light energy diffuses in the backward direction being blocked by the increasing potential barrier of the grating, which leads to a relatively smaller power required for RTL switching than for LTR switching.

In Fig. 5 we show the snapshots of the electric field for the RTL configuration with $L_0 = 200\Lambda$, $W_g = 0.1$ μm at the operating frequency 207.85 THz for (a) an off-state and (b) an on-state. Similar fields are observed for the case of the LTR configuration. From these figures it is found that the fields have a few peaks, which indicates that the mode of resonance in the grating is of higher-order. Due to both the strong grating modulation and the structural asymmetry, and despite that the incident light power has been gradually increased, the fundamental mode is not generated but the higher-order mode takes over. It has been found in our results that the off-state fields are significantly different between the RTL and the LTR (not shown) configurations. For the RTL configuration the field penetrates into the waveguide, while for the LTR configuration

#77312 - $15.00 USD Received 21 November 2006; revised 12 December 2006; accepted 13 December 2006

the field is blocked at the entrance to the waveguide. When the waveguide grating switches on, the field distributions become similar for the RTL and the LTR configurations.

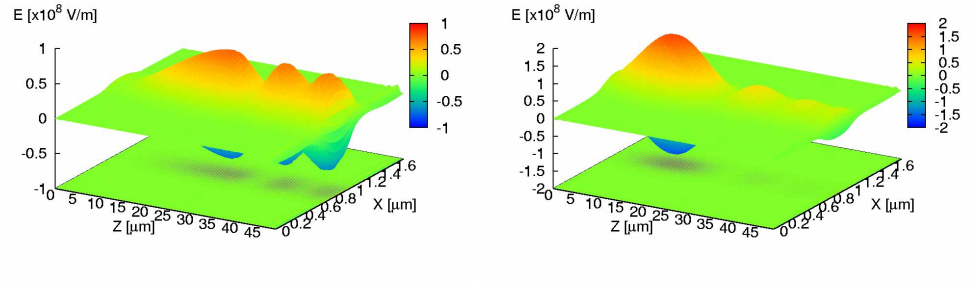

(a) (b)

Fig. 5. Electric field for 200Λ-long RTL configuration (positive variation) with $W_g = 0.1$ μm at 207.85 THz operating frequency. (a) off-state at 90 ps, and (b) on-state at 130 ps.

The relation between the length of the waveguide grating and the switching threshold for the RTL configuration is plotted in Fig. 6 with different operating frequencies $f_{op} = 207.85$ THz, 207.9 THz and 207.95 THz for $W_g = 0.1$ μm, and $f_{op} = 214.03$ THz for $W_g = 0.2$ μm as discussed later. The switching threshold no longer exhibits a linear dependence on the grating length when the grating is longer than approximately 210Λ. This behavior of the threshold value is considered to be due to the strong modulation of the grating. This tendency applies also to other cases of different W_g. The minimum threshold is obtained at length around 220Λ to 230Λ regardless of W_g. The WBGs longer than 235Λ are found unstable, causing a modulation-like field to grow rapidly, which is to be discussed in a later section. We have noted that for the minimum threshold condition at a length around 220Λ to 230Λ, the incident light and the light reflected from the grating become out of phase, and subsequently, the total field at the input port (right-hand-side port) becomes very small. Contrary, for shorter grating lengths the total field at the input port is observed significantly large (not shown). The total field near the input port will obviously affects the switching behavior. Therefore, the phase difference between the incident and the reflected lights, which is determined by the total length of the asymmetric grating, could be the main reason for the fact that the threshold is not linearly dependent on the grating length.

Next we further increase the sidewall modulation to $W_g = 0.20$ μm while maintaining the longitudinal profile of the modulation, i.e. the modulation amplitude $W_g/2$ of the grating varies according to the same polynomial, namely from 0.10 μm to 0.05 μm along the waveguide. The transmission spectra for the 200Λ-long asymmetric grating is compared with that of $W_g = 0.1$ μm in Fig. 3. The operating frequency for the nonlinear switching analysis was then chosen to be 214.03 THz, closer to the band edge (214.08 THz) than that of the previous case because the transmission spectrum is much steeper at the band edge, which allows the same level of extinction ratio for the nonlinear switching operation.

The results for the switching behavior are shown in Fig. 7. In this result the switching threshold has been reduced to $E_{th}^{(on)} = 1.05 \times 10^7$ V/m ($P_{th}^{(on)} = 77$ mW) for the RTL configuration, and to $E_{th}^{(on)} = 1.6 \times 10^7$ V/m ($P_{th}^{(on)} = 170$ mW) for the LTR configuration. In this case the switch-off threshold is not clearly visible, but it exists at around $E_{th}^{(off)} = 0.35 \times 10^7$ V/m for

#77312 - $15.00 USD Received 21 November 2006; revised 12 December 2006; accepted 13 December 2006

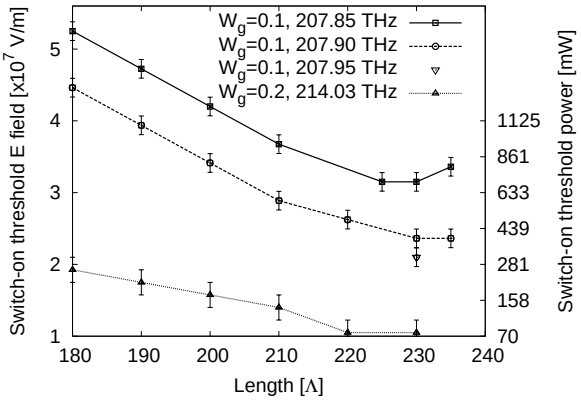

Fig. 6. Switch-on threshold electric field and power versus the length of the waveguide grating for the RTL (positive) configuration with $W_g = 0.1$ μm and 0.2 μm. The error bars are the uncertainty due to the step increment of the incident field variation.

both RTL and LTR. The time evolution exhibits larger fluctuations than that of the previous case in Fig. 4 because the operating frequency is closer to the band edge and therefore the extinction ratio is worse than that in Fig. 4. The change in normalized permittivity for the switch-on threshold is 3.6 $\times 10^{-5}$. Note that the transmission spectrum for $W_g = 0.20$ μm has a very steep transition and a large dip near the band edge, in comparison to those for $W_g = 0.10$ μm. However, we observe that the stability of the switching operation is not largely affected by the dip. The steep transition reduces the switch-on power significantly. If the switch turns on, the bandgap shifts to the lower frequency side, and the device can maintain the on-state like an electronic Schmitt trigger, irrespective of the fine structure of the transmission curve near the band edge.

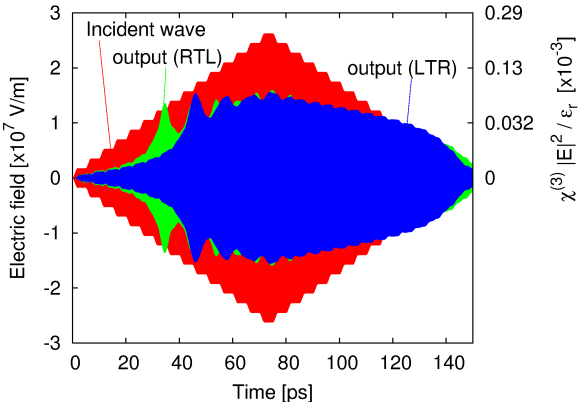

Fig. 7. Switching for the LTR and RTL configuration of a 220Λ-long waveguide with $W_g = 0.20$ μm at 214.03 THz operating frequency ($\Delta f = 0.05$ THz). Maximum incident field is 2.6×10^7 V/m at 75 ps. Minimum switch-on threshold is $E_{th}^{(on)} = 1.05 \times 10^7$ V/m ($P_{th}^{(on)} = 77$ mW) for RTL.

#77312 - $15.00 USD Received 21 November 2006; revised 12 December 2006; accepted 13 December 2006

As expected, the stronger modulation allows the reduction of the switching threshold significantly. With the incident laser power of 77 mW, the experimental observation of the switching operation in this device seems to be feasible. One may consider an alternate candidate for the nonlinear media, which would exist in a class of organic polymers; polydiacetylene 9-BCMU has a nonlinear susceptibility $\chi_0^{(3)} = 1.4 \times 10^{-16}$ m^2/V^2 [1]. This value is approximately 36 times larger than that of InGaAsP (Q1.35) investigated in this paper, and allows to reduce the required incident light power strongly, namely down to approximately 2 mW, which would enable an actual functional device having a very low threshold.

2.3. Stable state of nonlinear WBG

We have investigated the dynamic stability of an uniform WBG for comparison with the previous asymmetric WBGs. We observed a stable state for $L = 200\Lambda$, $W_g = 0.15\mu$m, uniform WBG at operating frequency 209.40 THz. The upper band-edge frequency of this structure is 209.55 THz. The time evolution of the field is shown in Fig. 8. In this case switching occurred at 40 ps with the incident threshold field $E_{th}^{(on)} = 1.6 \times 10^7$ V/m ($P_{th} = 170$ mW). For the time period between 40 ps and 50 ps, a relatively sharp pulse is observed. Further analyses showed that when the incident field is stronger the pulse becomes higher and narrower, leading to a number of soliton-like pulses generated and transmitted (not shown). After 50 ps, the incident power reduces gradually, and thereby the grating's inner field switches to a stable state, which is retained until the incident light almost vanishes at time 100 ps. The corresponding field distributions are shown in Fig. 9(a) for an off-state at 20 ps, and in (b) for an on-state at 60 ps. These field distributions clearly indicate that the field is of a longitudinal fundamental mode, because only a single envelope peak is observed for the on-state, which is similar to those observed in previous literature for 1D solutions [5, 10, 2]. Note that the field in Fig. 9(b) for the on-state is much larger than that in (a) for the off-state. It is also interesting to note in Fig. 8 that the on-state lasts for some picoseconds even after the incident light vanishes. This is a clear evidence of the fact that a large amount of energy is stored in the grating during the on-state, and once the incident light goes down across the switch-off threshold, the stored energy starts diffusing out of the grating. This diffusion process would take some picoseconds in this case. In addition, the switch-off threshold for this operation condition is significantly lower, which has extended the on-state duration even after the incident light has turned off. In general, for certain values of field amplitude and single-step risetime of the input-field staircase, it is possible that the system prefers to stay in the transmitting on-state by exciting gap solitons and by radiating the excess energy as a train of pulses ([10] Fig.3). Such a gap soliton may be observed at time 60 ps in Fig. 8, where the field distribution resembles that of a soliton, Fig. 9(b). This stable gap soliton decays relatively slowly, even if the input pulse falls below the switch-off threshold.

2.4. Pulsative state of nonlinear WBG

Interestingly, for the same analysis conditions as the previous taper configuration of $W_g = 0.2$ μm except that the grating modulation is uniform, the stable switching is not observed clearly even when a relatively high-power incident light is launched. Instead, a pulsative state is suddenly observed as shown in Fig. 10. By comparison with the results for the asymmetric WBG in Fig. 7, it is found that the asymmetric grating has an effect of stabilizing the switch-on state. Similar stability characteristics have been investigated by Jia et.al. for a weakly-modulated-taper nonlinear Erbium-doped fiber Bragg grating [9]. According to their results, stability of Bragg grating structures is significantly affected by the taper configuration of the grating, and it is indeed not straightforwardly predictable. In our WBG structure the grating modulation is much stronger, and thereby the stability range is even more reduced. Without the gradual change of the electric field modulation, the transition between the stable and the pulsative states is so

#77312 - $15.00 USD Received 21 November 2006; revised 12 December 2006; accepted 13 December 2006

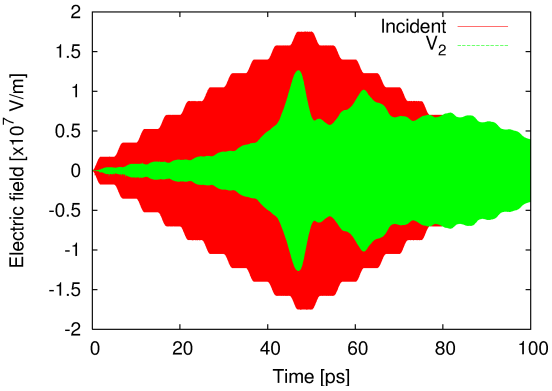

Fig. 8. An example of the stable switching state for a uniformly modulated WBG of 200Λ in length, $W_g = 0.15\mu$m at operating frequency 209.40 THz ($\Delta f = 0.15$ THz). The maximum field is 1.75 $\times 10^7$ V/m. Switch-on occurs at $E_{th}^{(on)} = 1.6 \times 10^7$ V/m ($P_{th}^{(on)} = 170$ mW).

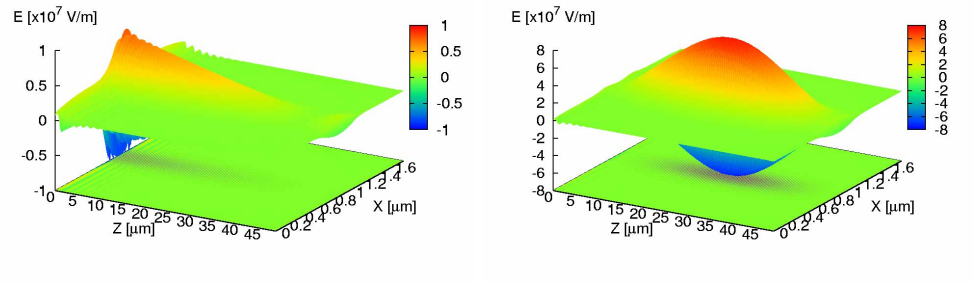

(a) (b)

Fig. 9. Stable state electric field for 200Λ-long uniform grating. $W_g = 0.15\mu$m, 209.40 THz, 1.75 $\times 10^7$ V/m. (a) off-state at 20 ps, and (b) on-state at 60 ps.

sudden that the stable distribution of the field is hardly retained in the WBG structure. This explanation is consistent with the transmission spectrum (Fig. 3) that has a very steep transition and a large dip at higher-frequency side of the first peak near the upper band edge. It is therefore anticipated that the switching property would be improved by a careful design of the grating configuration.

2.5. Chaotic state of nonlinear WBG

It was found that when the waveguide was longer than a certain length the nonlinear analysis tends to diverge at a relatively small incident field, resulting in a modulation-like behavior, and finally resulting in a chaotic state. The similar phenomena have also been reported elsewhere [6, 8]. In the discussion of the stability characteristics of Bragg gratings by Jia et.al. [9], it is shown that the modulation instability occurs in nonlinear Bragg gratings due to the interplay between group velocity dispersion (GVD) and nonlinear effects. This mechanism is close to that

#77312 - $15.00 USD Received 21 November 2006; revised 12 December 2006; accepted 13 December 2006

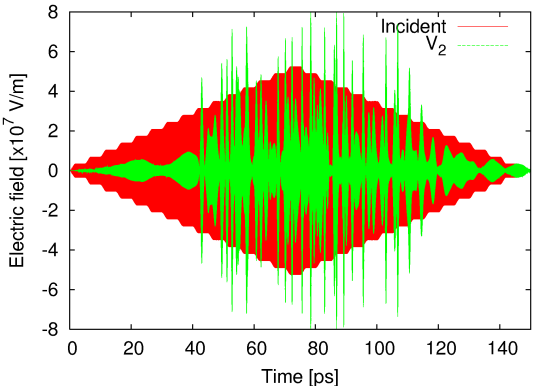

Fig. 10. An example of the pulsative time signal for a uniformly modulated WBG of 220Λ in length, $W_g = 0.2\mu$m at operating frequency 214.03 THz ($\Delta f = 0.05$ THz). The maximum incident field is 5.25 $\times 10^7$ V/m. Transition to the pulsative state occurs at incident field $E =$ 3.2 $\times 10^7$ V/m (equivalent power $P = 720$ mW).

of the optical soliton propagation and self-focusing phenomena, as it has been demonstrated numerically using the same FDTD algorithm [18]. Due to even stronger dispersion in a Bragg grating at a frequency close to its band edge, the onset of modulation instability occurs at a lower power level for Bragg gratings in comparison to solitons in an ordinary waveguide. The chaotic behavior following the self-focusing of a light beam has been investigated using a soft-core Coulomb potential (SCP) model of bound electrons [16]. We show here that the SCP is applicable to nonlinear Bragg gratings for the investigation of the dynamic chaotic behavior of the grating field.

The SCP model can avoid the singularity of an instantaneous nonlinearity by employing a saturation mechanism near the core of a Coulomb potential; the binding force of an atom is derived from the so-called soft-core Coulomb potential [16]

$$U(x) = -\frac{q^2}{\sqrt{a_0^2 + x^2}}\,, \tag{2}$$

where x is the displacement from equilibrium for a bound particle having an electric charge q, and a_0 is an equiliblium radius. These parameters can be determined from desired nonlinear properties such as linear sceptibility, third-order nonlinear sceptibility, and a characteristic resonance frequency of the charged particle. In its differential equation of electron motion it has a term for the Lorentz dispersion and a term for the 3rd-order nonlinearity, which can be efficiently implemented in the FDTD algorithm through the ADE formalism [18]. We will report the detailed analysis in a forthcoming paper.

In Fig. 11 we show the time evolution of the field detected at the input port V_1 and at the output port V_2, for a uniformly modulated WBG of 300Λ in length; (a) is for the instantaneous Kerr nonlinearity and the Lorentz dispersion with a damping factor $\delta_p = 1.0 \times 10^{14}$ rad/s, and (b) for the SCP model with a damping factor $\delta_p = 1.0 \times 10^{13}$ rad/s. From these results one can see that the SCP model allows the observation of the chaotic behavior, at least qualitatively, by virtue of the saturating nature of the model, while in (a) even with a larger damping factor the calculation stops due to a convergence problem of the nonlinear algorithm. Our extensive study shows that when the damping factor is increased for the Lorentz dispersion model, the

#77312 - $15.00 USD Received 21 November 2006; revised 12 December 2006; accepted 13 December 2006

modulation-like field builds up like the result in (a) at a slightly later time, and it results in the same convergence problem of the nonlinear algorithm.

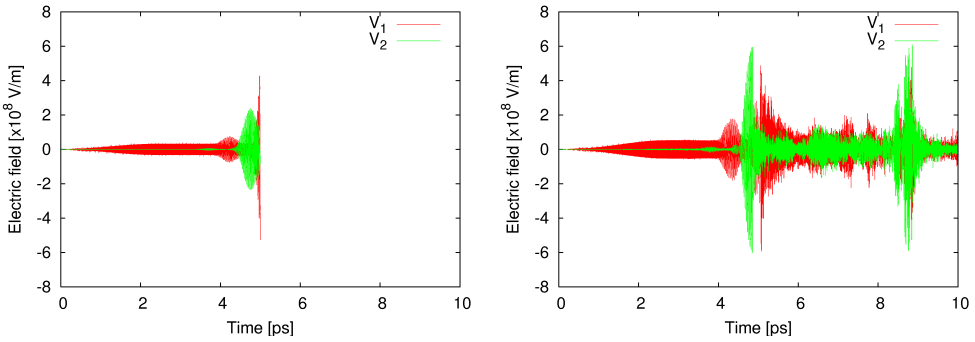

(a) Optical Kerr model for $f_{op} = 206.5$ THz ($\Delta f = 0.2$ THz), with Lorentz dispersion with the damping factor $\delta_p = 1.0 \times 10^{14}$ rad/s. Calculation stopped at 5 ps.

(b) SCP model for $f_{op} = 200.3$ THz ($\Delta f = 0.2$ THz), with the damping factor $\delta_p = 1.0 \times 10^{13}$ rad/s. Calculation still continues after 10 ps.

Fig. 11. Time signals that exhibit the modulation-like instability. For uniform WBGs of $L_0 = 300\ \Lambda$. The incident light is a smoothly excited sinusoid with the maximum field 5.25 $\times\ 10^7$ V/m.

3. Conclusions

We have demonstrated numerically non-reciprocal transmission and Schmitt trigger operation in asymmetric WBGs with strong sidewall modulation. The asymmetric WBG structure exhibits a stable switching region at the incident light power as small as 77 mW for the RTL configuration (positively varying stopband) and 170 mW for the LTR configuration (negatively varying stopband). This threshold power is in a level experimentally accessible in an actual functional device. We have also demonstrated the analysis of stable, pulsative, and chaotic states of the nonlinear WBG structure with the FDTD method. In particular, it is found that asymmetricity of WBGs allows a stable switching operation compared to uniformly modulated WBGs. The modulation-like instability is qualitatively investigated by using a numerically stable nonlinear algorithm based on the soft-core Coulomb potential model.

Acknowledgements

This work was supported in part by the Deutsche Forschungsgemeinschaft (DFG) Research Training Group 786 “Mixed Fields and nonlinear interactions” at the University of Karlsruhe, and in part by the Center for Functional Nanostructures (CFN) of the DFG within project A3.1.

M.F acknowledges the R&D promotion scheme funding international joint research by the National Institute of information and Communications Technology (NICT), Japan, and the Scientific Research Grant in Aid from the Japan Society for the promotion of Science (JSPS).